Bidirectional dynamic scaling in an isolated Bose gas far from equilibrium

Jake A. P. Glidden,[1,*] Christoph Eigen,[1] Lena H. Dogra,[1] Timon A. Hilker,[1] Robert P. Smith,[2] and Zoran Hadzibabic[1,†]

[1]*Cavendish Laboratory, University of Cambridge, J. J. Thomson Avenue, Cambridge CB3 0HE, United Kingdom*
[2]*Clarendon Laboratory, University of Oxford, Parks Road, Oxford OX1 3PU, United Kingdom*

Understanding and classifying nonequilibrium many-body phenomena, analogously to the classification of equilibrium states of matter into universality classes[1,2], is an outstanding problem in physics. From stellar matter to financial markets, any many-body system can be out of equilibrium in a myriad of ways, and many are difficult to experiment on. It is therefore a major goal to establish universal principles that apply to different phenomena and physical systems. For equilibrium states, the universality seen in the self-similar spatial scaling of systems close to phase transitions lies at the heart of their classification. Recent theoretical work[3–14] and experimental evidence[15,16] suggest that isolated many-body systems far from equilibrium generically exhibit dynamic (spatiotemporal) self-similar scaling, akin to turbulent cascades[17] and the Family–Vicsek scaling in classical surface growth[18,19]. Here we observe bidirectional dynamic scaling in an isolated quench-cooled atomic Bose gas; as the gas thermalises and undergoes Bose–Einstein condensation, it shows self-similar net flows of particles towards the infrared (smaller momenta) and energy towards the ultraviolet (smaller lengthscales). For both infrared and ultraviolet dynamics we find that the scaling exponents are independent of the strength of the interparticle interactions that drive the thermalisation.

A key question in the quest to understand nonequilibrium dynamics is how an isolated quantum many-body system that is initially far from equilibrium thermalises[20,21]; experiments on ultracold atomic gases[22] have investigated various aspects of this problem, through studies of, e.g., integrability[23], prethermalization[24,25], generalised Gibbs ensembles[26], and the Eigenstate Thermalisation Hypothesis[27]. Possible universal features of far-from-equilibrium thermalisation have recently been conceptualised in the framework of so-called non-thermal fixed points (NTFPs)[4]. Qualitatively, the expectation is that an isolated far-from-equilibrium system 'struggles to find its way home' and shows spatiotemporal power-law scaling rather than exponential relaxation towards equilibrium. Analogously to the critical slowing down near an equilibrium critical point, such behaviour is associated with the system being attracted to an NTFP and spending a lot of time near it, and is insensitive to both initial conditions and microscopic details of the system. This type of spatiotemporal scaling has been predicted to occur in diverse contexts including ultracold atomic gases[7–10], quantum magnets[12], and the quark-gluon plasma[7,8,13]. In the context of ultracold atoms, these theories give a new perspective to the foundational[28–38] and still open[39,40] problem of the formation of a Bose–Einstein condensate (BEC).

First experimental evidence for the emerging NTFP paradigm was seen in one-dimensional (1D) harmonically trapped atomic gases[15,16]. So far, self-similar scaling was observed only in the infrared dynamics. Our experiments reveal both infrared (IR) and ultraviolet (UV) spatiotemporal scaling in the textbook setting of a homogeneous 3D Bose gas[41], with tuneable interactions and near-perfect isolation from the environment.

The idea of our experiments is depicted in Fig. 1a. We start with an equilibrium homogeneous ^{39}K gas of $N \approx 1.2 \times 10^5$ atoms in the lowest hyperfine ground state, confined in a cylindrical optical box[42] of diameter $D \approx 27\,\mu\mathrm{m}$, length $L \approx 46\,\mu\mathrm{m}$, and depth $U_\mathrm{D} \approx k_\mathrm{B} \times 1\,\mu\mathrm{K}$. The tuneable interactions in our gas are characterised by the scattering length a. Initially $a = 200\,a_0$, where a_0 is the Bohr radius, and $T \approx 130\,\mathrm{nK}$, just above the condensation temperature T_c. We then create a far-from-equilibrium cloud by removing 77 % of the atoms and 97.5 % of the total energy E, so the energy per particle drops by an order of magnitude, and in equilibrium the gas would be (partially) condensed. Using tuneable interactions allows us to completely separate this quench from the subsequent equilibration. First, we switch off the interactions (tune $a \to 0$) and then lower U_D to $k_\mathrm{B} \times 30\,\mathrm{nK}$ for 2 s, so high energy atoms escape without the remaining ones thermalising; this results in a far-from-equilibrium momentum distribution n_k. Then, only after closing the system by raising U_D, we turn on the interactions (within a few milliseconds) and thus start the clock for thermalisation. To probe the state of the gas after a variable relaxation time t, we turn off both the trap and the interactions, and infer $n_k(k,t)$ from absorption images taken after ballistic expansion of the cloud (see Methods).

As shown in Fig. 1b, during thermalisation (at $300\,a_0$) the total N and E remain constant. In Fig. 1c we plot both the spectral population density $\mathcal{N}_k = 4\pi k^2 n_k$ (left) and the spectral energy density $\mathcal{E}_k = \mathcal{N}_k \hbar^2 k^2/(2m)$ (right); here the conserved N and E, respectively, correspond to the areas under the curves. As indicated by the arrows, we observe bidirectional dynamics in momentum space[30]: while the majority of atoms flows to the IR, where the condensate emerges, the energy, carried by a small fraction of atoms, flows to the UV. In Fig. 1d we plot two different apparent temperatures, T_peak and T_low, both deduced from $\mathcal{E}_k$ by (incorrectly) assuming equilibrium. For an equilibrium gas, at $T \leq T_\mathrm{c}$, one can simply get T from k_peak, the momentum where $\mathcal{E}_k$ peaks, but alternatively one can consider only the low-k states, where $\mathcal{E}_k \propto Tk^2$ for $k \to 0$. Here, the apparent $T_\mathrm{peak} \propto k_\mathrm{peak}^2$ is initially far below the equilibrium temperature, $T_\mathrm{eq} \approx 32\,\mathrm{nK}$, corresponding to the conserved E (see Methods). On the

* email: japg2@cam.ac.uk
† email: zh10001@cam.ac.uk

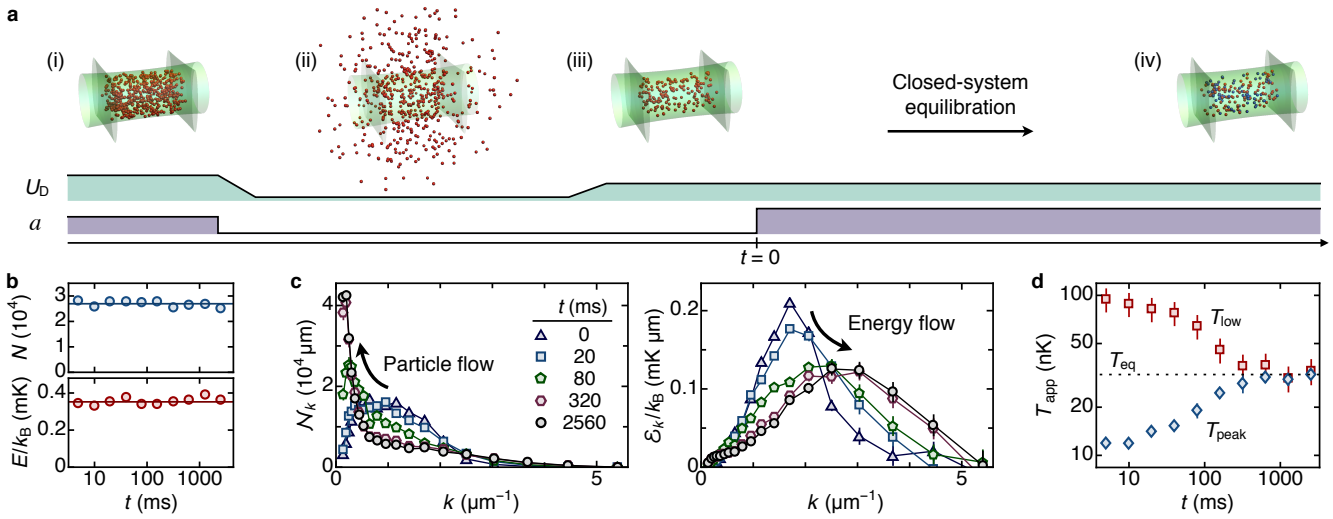

Fig. 1 | Bidirectional thermalisation in an isolated gas. a, Experimental protocol; U_D is the depth of the optical box trap (green) and a the scattering length characterising interactions. (i) We prepare an equilibrium cloud of $N \approx 1.2 \times 10^5$ atoms at $T \approx 130\,\mathrm{nK}$, just above the condensation temperature. (ii) We turn off the interactions ($a \to 0$) and then lower U_D, so high energy atoms escape without the remaining ones thermalising. (iii) We close the system by raising U_D and then initiate thermalisation, at $t = 0$, by tuning a to a nonzero value. (iv) Equilibrium state, with both thermal (red) and condensed (blue) components. **b - d,** Thermalisation at $a = 300\,a_0$. **b,** Total atom number, N, and energy, E, remain constant. **c,** Evolution of the spectral distributions of particles, $\mathcal{N}_k$, and energy, $\mathcal{E}_k$; the net particle flow is to the IR and the net energy flow to the UV. **d,** The low-k behaviour of $\mathcal{E}_k$ and the momentum where $\mathcal{E}_k$ peaks show different apparent temperatures (T_{low} and T_{peak}, respectively), which converge to the expected equilibrium temperature T_{eq} on similar timescales. In **b - d**, error bars show 1 s.e.m. (not visible when smaller than the symbol size); error bars for T_{low} include an additional contribution from the volume uncertainty.

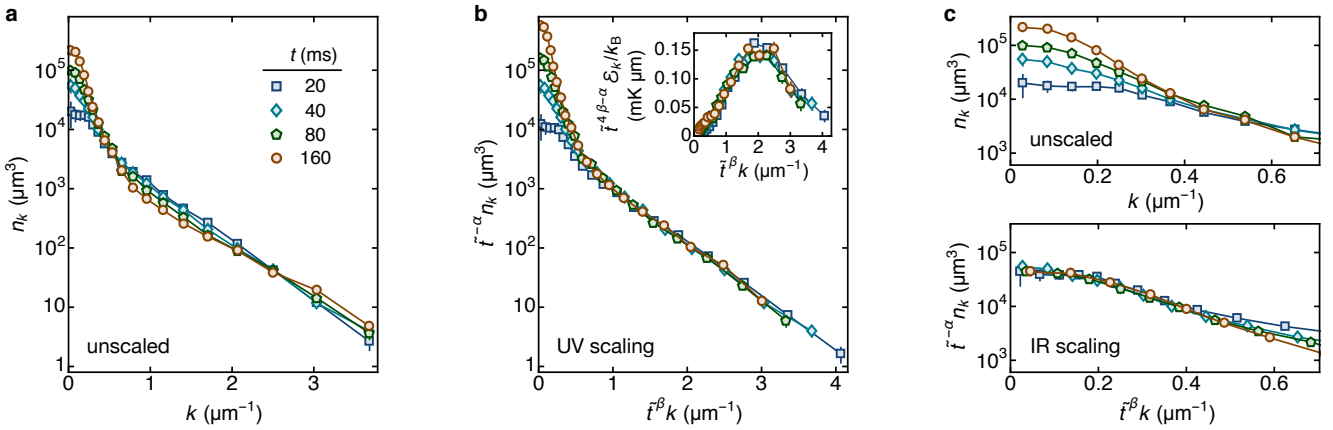

Fig. 2 | Self-similar scaling dynamics. Here $a = 300\,a_0$ during closed-system thermalisation. For scaling n_k according to Eq. (1), we arbitrarily set $t_0 = 40\,\mathrm{ms}$. **a,** Unscaled n_k curves; the legend applies to all panels. Note that the inverse healing length is $k_\xi = \sqrt{8\pi n a} \approx 0.7\,\mu\mathrm{m}^{-1}$, where n is the real-space density. **b,** UV scaling, with $\alpha = -0.70(7)$ and $\beta = -0.14(2)$, collapses the curves for $\tilde{t}^\beta k \gtrsim 1\,\mu\mathrm{m}^{-1}$. The inset shows the scaled $\mathcal{E}_k$ curves, for comparison with Fig. 1c. Here $\alpha/\beta \approx 5$, consistent with energy-conserving transport. **c,** IR scaling. Top panel: a zoom-in on the unscaled n_k curves at low k. Bottom panel: scaling with $\alpha = 1.15(8)$ and $\beta = 0.34(5)$ collapses the curves for $\tilde{t}^\beta k \lesssim 0.5\,\mu\mathrm{m}^{-1}$. Now $\alpha/\beta \approx 3$, consistent with particle-conserving transport. All error bars show 1 s.e.m. (not visible when smaller than the symbol size).

other hand, the low-k T_{low} is initially far above T_{eq} (and close to the pre-quench temperature). The two apparent temperatures thus evolve in opposite directions, and we find that they converge to T_{eq} on similar timescales.

The universal-scaling prediction is that at intermediate times, when the state of the system is distinct from both the initial and the final (equilibrium) one, the thermalisation dynamics can in some appropriate (IR and UV) momentum ranges be described by spatiotemporal scaling of the form

$$n_k(\mathbf{k}, t) = \tilde{t}^{\alpha}\, n_k(\tilde{t}^{\beta}\mathbf{k}, t_0), \tag{1}$$

where t_0 is a reference time, $\tilde{t} = t/t_0$, and the scaling exponents α and β are positive (negative) for transport towards the IR (UV). This implies that the n_k distributions at different times can, separately in the IR and the UV, be collapsed onto universal curves. It also suggests a similarity to self-similar turbulent cascades[43–45]; see also ref. [30].

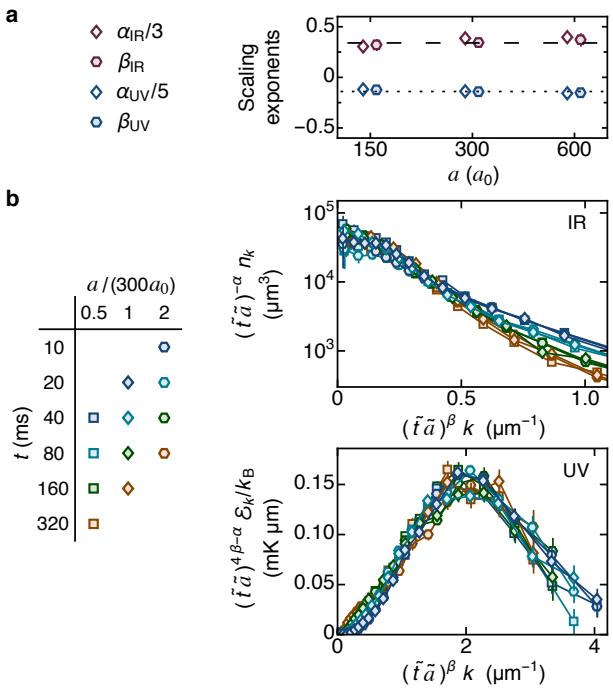

Fig. 3 | Universality for different interaction strengths. **a,** Scaling exponents are insensitive to the value of a during thermalisation; the α and β points are slightly offset horizontally for visual clarity. The dashed and dotted lines, respectively, show $\beta_{IR} = 0.34$ and $\beta_{UV} = -0.14$. **b,** Generalising $t \to t\tilde{a}$ in Eq. (1) collapses (separately in the IR and the UV) all curves taken within the scaling interval $t\tilde{a} \in [20\,\text{ms}, 160\,\text{ms}]$; here $\tilde{a} = a/(300\,a_0)$, where $300\,a_0$ is an arbitrary reference point. All error bars reflect 1 s.e.m. (not visible when smaller than the symbol size).

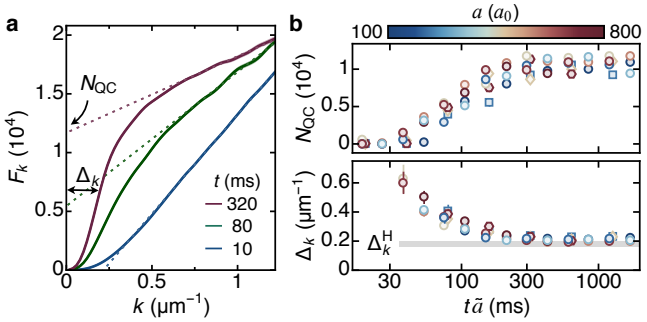

Fig. 4 | Quasi-condensation and phase ordering. a, We extract the quasi-condensate atom number, N_{QC}, and momentum-space width, Δ_k, from the cumulative particle distribution F_k (see text); here $a = 300\,a_0$. Standard errors in F_k are smaller than the line thickness. **b,** Evolution of N_{QC} and Δ_k for various interaction strengths is given by universal curves when plotting versus $t\tilde{a}$. The error bars (not visible when smaller than the symbol size) reflect fitting errors. At long times Δ_k approaches the Heisenberg limit Δ_k^H (horizontal bar), corresponding to a fully coherent condensate.

The bidirectional dynamics in our gas indeed show such spatiotemporal scaling. Specifically, for $a = 300\,a_0$ (as in Fig. 1), we observe dynamic scaling for $t \in [20\,\text{ms}, 160\,\text{ms}]$. In Fig. 2a we show the unscaled $n_k(t)$ curves. For the scaled ones in Fig. 2b,c we arbitrarily set $t_0 = 40\,\text{ms}$ and have optimised their collapse by varying α and β (see Methods).

In Fig. 2b we see UV scaling in a broad momentum range $\tilde{t}^{\beta}k \gtrsim 1\,\mu\text{m}^{-1}$, with $\alpha = -0.70(7)$ and $\beta = -0.14(2)$. In the inset we show the scaled $\mathcal{E}_k$ curves, which highlight variations in the UV and can be directly compared with the unscaled curves in Fig. 1c. The ratio of the scaling exponents, $\alpha/\beta \approx 5$, is consistent with energy-conserving transport; for particles with a quadratic dispersion relation in d dimensions, one expects $\alpha/\beta = d$ for a particle-conserving transport and $\alpha/\beta = d + 2$ for an energy-conserving one (see, e.g., refs. [9,11]).

In Fig. 2c we focus on the complementary IR k-range, and show both unscaled (top) and scaled (bottom) distributions. Here we observe collapse for $\tilde{t}^{\beta}k \lesssim 0.5\,\mu\text{m}^{-1}$, with $\alpha = 1.15(8)$ and $\beta = 0.34(5)$, and $\alpha/\beta \approx 3$ consistent with particle-conserving transport.

We next explore the generalisation of universal dynamics to different interaction strengths (see Fig. 3), by repeating analogous experiments with $a = 150\,a_0$ and $600\,a_0$ during thermalisation at $t > 0$. We find that all our results remain essentially the same if we rescale the thermalisation clock by $t \to t\tilde{a}$, where $\tilde{a} = a/(300\,a_0)$; $t_0 = 40\,\text{ms}$ throughout. For all a, we observe scaling dynamics in the interaction-normalised interval $t\tilde{a} \in [20\,\text{ms}, 160\,\text{ms}]$, and find very similar scaling exponents, summarised in Fig. 3a; combining all our data gives $\alpha_{IR} = 1.08(9)$, $\beta_{IR} = 0.34(4)$, $\alpha_{UV} = -0.67(6)$, and $\beta_{UV} = -0.14(2)$. In Fig. 3b we show that, both in the IR and in the UV, generalising $t \to t\tilde{a}$ in Eq. (1) collapses all our different-a curves taken within the scaling $t\tilde{a}$-interval; here we use our a-averaged scaling exponents, and for visual clarity in the UV we show scaled $\mathcal{E}_k$ curves. We have also considered a more general interaction-scaling $t \propto a^{-p}$ and optimised the collapse of the curves in Fig. 3b with respect to p; this gave $p_{IR} = 0.9(1)$ and $p_{UV} = 1.1(1)$.

The $1/a$ scaling of the characteristic timescales implies that they are set by the inverse interaction energy, rather than the inverse two-body scattering rate, $\propto 1/a^2$; see ref. [39] for an overview of long-standing discussions on this issue. Defining the characteristic time set by the inverse interaction energy, $\tau = \hbar/(gn)$, where $g = 4\pi\hbar^2 a/m$ and n is the real-space particle density, the scaling interval $t\tilde{a} \in [20\,\text{ms}, 160\,\text{ms}]$ for all a corresponds to $t \in [8.5\,\tau, 68\,\tau]$.

Finally, we look at the properties of the condensate that emerges during thermalisation. The IR scaling in Figs. 2 and 3, seen for all low k, implies that the characteristic momentum width of the condensate, Δ_k, is reducing. This is not consistent with a fully coherent BEC, which has a fixed Heisenberg-limited width Δ_k^H set by the system size[46], with $\Delta_k^H \to 0$ in the thermodynamic limit. However, it is consistent with the emergence of an out-of-equilibrium quasi-condensate (QC) that is initially riddled with excitations such as vortex loops[36,47] or domain walls[48], and has $\Delta_k > \Delta_k^H$. Generally, Δ_k^{-1} is a characteristic coherence length (limited by system size), and only with full phase-ordering $\Delta_k \to \Delta_k^H$.

Inspired by ref. [36], we define the quasi-condensate atom number, N_{QC}, and width, Δ_k, as illustrated in Fig. 4a. Here, $F_k(k) = \int_0^k \mathcal{N}_k(k')\mathrm{d}k'$ is the cumulative atom distribu-

tion. In the thermodynamic limit, for an ideal equilibrium gas of (large) volume V and with N_0 condensed atoms, $F_k = N_0 + bTk$ for $k \to 0$, where $b = Vmk_B/(\pi^2\hbar^2)$; in this case the BEC is localised in $k = 0$ and the low-k contribution of the saturated thermal gas to F_k is $\propto Tk$ because in the classical-field regime $\mathcal{N}_k \propto T$ is k-independent. In a finite-size and/or nonequilibrium gas, the (quasi-)condensate contribution to F_k is spread over $\sim \Delta_k$, but in its presence one can still see a low-k 'shoulder' in F_k and the linear regime at slightly larger k (around $1\,\mu\mathrm{m}^{-1}$ in Fig. 4a); here the slope in the linear regime corresponds to T_{low} in Fig. 1d. We linearly fit the data for $k > 0.8\,\mu\mathrm{m}^{-1}$ (dotted lines) and define N_{QC} by the positive intercept of this fit, while negative intercepts mean $N_{\mathrm{QC}} = 0$. Finally, we define Δ_k as the k-range containing half of N_{QC}, which for our system gives $\Delta_k^{\mathrm{H}} = 0.18(2)\,\mu\mathrm{m}^{-1}$ (see Methods).

In Fig. 4b we show how N_{QC} and Δ_k evolve and eventually, at times beyond the scaling interval $t\tilde{a} \in [20\,\mathrm{ms}, 160\,\mathrm{ms}]$, approach their equilibrium values. Here we include additional data taken for various a in the range $(100 - 800)\,a_0$, which all fall onto universal curves when plotted versus $t\tilde{a}$. The QC emerges soon after the start of thermalisation, since our pre-quench gas is close to condensation, but initially Δ_k is notably above the Heisenberg limit. At long times, the condensed fraction N_{QC}/N approaches $40(5)\,\%$, consistent with the conserved N and E shown in Fig. 1b (see Methods), while Δ_k approaches the Heisenberg limit, corresponding to a fully coherent BEC. The phase-ordering corresponding to the Δ_k decrease is reminiscent of the domain-coarsening one expects after a (relatively slow) Kibble–Zurek-style quench of temperature through the critical point[48]. However, in the Kibble–Zurek picture the phase-ordering lags behind the quasi-condensate formation (which occurs already during the quench), while here we observe concurrent N_{QC} growth and Δ_k decrease.

Our experiments provide a comprehensive picture of the universal bidirectional dynamic scaling in an isolated quantum gas, quasi-condensation, and phase ordering. They also raise questions for further theoretical and experimental work. The observed ratios of scaling exponents, α/β, confirm the expectations linked to fundamental conservation laws. On the other hand, the values of the individual exponents are still subject of extensive theoretical work, for which our experiments provide invaluable benchmarks. For the UV dynamics, our $\beta_{\mathrm{UV}} = -0.14(2)$ is close to the prediction for weak-wave turbulence[17,43], $\beta_{\mathrm{UV}} = -1/6$. For the IR dynamics, NTFP theories[7–11] generally predict $\beta_{\mathrm{IR}} = 1/2$, but recent work[10,11] also suggests the possibility of $\beta_{\mathrm{IR}} = 1/3$, closer to our $\beta_{\mathrm{IR}} = 0.34(6)$; in the future it would be interesting to explore the conditions under which either might be observed. Finally, it would also be interesting to perform similar quench experiments starting far above T_{c}, since the dynamics on the way to (quasi-)condensation and following its onset are expected to be different[39].

References

1. P. C. Hohenberg and B. I. Halperin, "Theory of dynamic critical phenomena," Rev. Mod. Phys. **49**, 435–479 (1977).
2. P. M. Chaikin and T. C. Lubensky, *Principles of Condensed Matter Physics* (Cambridge University Press, 1995).
3. R. Micha and I. I. Tkachev, "Turbulent thermalization," Phys. Rev. D **70**, 043538 (2004).
4. J. Berges, A. Rothkopf, and J. Schmidt, "Nonthermal Fixed Points: Effective Weak Coupling for Strongly Correlated Systems Far from Equilibrium," Phys. Rev. Lett. **101**, 041603 (2008).
5. B. Nowak, J. Schole, D. Sexty, and T. Gasenzer, "Nonthermal fixed points, vortex statistics, and superfluid turbulence in an ultracold Bose gas," Phys. Rev. A **85**, 043627 (2012).
6. B. Nowak, J. Schole, and T. Gasenzer, "Universal dynamics on the way to thermalization," New J. Phys. **16**, 093052 (2014).
7. J. Berges, K. Boguslavski, S. Schlichting, and R. Venugopalan, "Universality Far from Equilibrium: From Superfluid Bose Gases to Heavy-Ion Collisions," Phys. Rev. Lett. **114**, 061601 (2015).
8. A. Piñeiro Orioli, K. Boguslavski, and J. Berges, "Universal self-similar dynamics of relativistic and nonrelativistic field theories near nonthermal fixed points," Phys. Rev. D **92**, 025041 (2015).
9. I. Chantesana, A. Piñeiro Orioli, and T. Gasenzer, "Kinetic theory of nonthermal fixed points in a Bose gas," Phys. Rev. A **99**, 043620 (2019).
10. A. N. Mikheev, C.-M. Schmied, and T. Gasenzer, "Low-energy effective theory of nonthermal fixed points in a multicomponent Bose gas," Phys. Rev. A **99**, 063622 (2019).
11. C.-M. Schmied, A. N. Mikheev, and T. Gasenzer, "Nonthermal fixed points: Universal dynamics far from equilibrium," Int. J. Mod. Phys. A **34**, 1941006 (2019).
12. S. Bhattacharyya, J. F. Rodriguez-Nieva, and E. Demler, "Universal dynamics far from equilibrium in Heisenberg ferromagnets," arXiv:1908.00554 (2019).
13. J. Berges, K. Boguslavski, M. Mace, and J. M. Pawlowski, "Gauge-invariant condensation in the nonequilibrium quark-gluon plasma," Phys. Rev. D **102**, 034014 (2020).
14. K. Fujimoto, R. Hamazaki, and Y. Kawaguchi, "Family-Vicsek Scaling of Roughness Growth in a Strongly Interacting Bose Gas," Phys. Rev. Lett. **124**, 210604 (2020).
15. M. Prüfer, P. Kunkel, H. Strobel, S. Lannig, D. Linnemann, C.-M. Schmied, J. Berges, T. Gasenzer, and M. K. Oberthaler, "Observation of universal dynamics in a spinor Bose gas far from equilibrium," Nature **563**, 217–220 (2018).
16. S. Erne, R. Bücker, T. Gasenzer, J. Berges, and J. Schmiedmayer, "Universal dynamics in an isolated one-dimensional Bose gas far from equilibrium," Nature **563**, 225–229 (2018).
17. V. E. Zakharov, V. S. L'vov, and G. Falkovich, *Kolmogorov spectra of turbulence* (Springer Berlin, 1992).
18. F. Family and T. Vicsek, "Scaling of the active zone in the Eden process on percolation networks and the ballistic deposition model," J. Phys. A **18**, L75–L81 (1985).
19. M. Kardar, G. Parisi, and Y.-C. Zhang, "Dynamic scaling of growing interfaces," Phys. Rev. Lett. **56**, 889–892 (1986).
20. A. Polkovnikov, K. Sengupta, A. Silva, and M. Vengalattore, "*Colloquium* : Nonequilibrium dynamics of closed interacting quantum systems," Rev. Mod. Phys. **83**, 863–883 (2011).
21. C. Gogolin and J. Eisert, "Equilibration, thermalisation, and the emergence of statistical mechanics in closed quantum systems," Rep. Prog. Phys. **79**, 056001 (2016).
22. T. Langen, R. Geiger, and J. Schmiedmayer, "Ultracold Atoms Out of Equilibrium," Annu. Rev. Condens. Matter Phys. **6**, 201–217 (2015).
23. T. Kinoshita, T. Wenger, and D. S. Weiss, "A quantum Newton's cradle," Nature **440**, 900–903 (2006).
24. M. Gring, M. Kuhnert, T. Langen, T. Kitagawa, B. Rauer, M. Schreitl, I. Mazets, D. A. Smith, E. Demler, and J. Schmied-

mayer, "Relaxation and Prethermalization in an Isolated Quantum System," Science **337**, 1318–1322 (2012).
25. C. Eigen, J. A. P. Glidden, R. Lopes, E. A. Cornell, R. P. Smith, and Z. Hadzibabic, "Universal prethermal dynamics of Bose gases quenched to unitarity," Nature **563**, 221–224 (2018).
26. T. Langen, S. Erne, R. Geiger, B. Rauer, T. Schweigler, M. Kuhnert, W. Rohringer, I. E. Mazets, T. Gasenzer, and J. Schmiedmayer, "Experimental observation of a generalized Gibbs ensemble," Science **348**, 207–211 (2015).
27. A. M. Kaufman, M. E. Tai, A. Lukin, M. Rispoli, R. Schittko, P. M. Preiss, and M. Greiner, "Quantum thermalization through entanglement in an isolated many-body system," Science **353**, 794–800 (2016).
28. D. W. Snoke and J. P. Wolfe, "Population dynamics of a Bose gas near saturation," Phys. Rev. B **39**, 4030–4037 (1989).
29. H. T. C. Stoof, "Formation of the Condensate in a Dilute Bose Gas," Phys. Rev. Lett. **66**, 3148–3151 (1991).
30. B. V. Svistunov, "Highly nonequilibrium Bose condensation in a weakly interacting gas," J. Moscow Phys. Soc. **1**, 373–390 (1991).
31. Yu. M. Kagan, B. V. Svistunov, and G. V. Shlyapnikov, "Kinetics of Bose condensation in an interacting Bose gas," Sov. Phys. JETP **75**, 387–393 (1992).
32. D. V. Semikoz and I. I. Tkachev, "Kinetics of Bose Condensation," Phys. Rev. Lett. **74**, 3093–3097 (1995).
33. Yu. Kagan, G. V. Shlyapnikov, and J. T. M. Walraven, "Bose–Einstein Condensation in Trapped Atomic Gases," Phys. Rev. Lett. **76**, 2670–2673 (1996).
34. K. Damle, S. N. Majumdar, and S. Sachdev, "Phase ordering kinetics of the Bose gas," Phys. Rev. A **54**, 5037–5041 (1996).
35. C. W. Gardiner, P. Zoller, R. J. Ballagh, and M. J. Davis, "Kinetics of Bose–Einstein Condensation in a Trap," Phys. Rev. Lett. **79**, 1793–1796 (1997).
36. N. G. Berloff and B. V. Svistunov, "Scenario of strongly nonequilibrated Bose–Einstein condensation," Phys. Rev. A **66**, 013603 (2002).
37. H.-J. Miesner, D. M. Stamper-Kurn, M. R. Andrews, D. S. Durfee, S. Inouye, and W. Ketterle, "Bosonic Stimulation in the Formation of a Bose–Einstein Condensate," Science **279**, 1005–1007 (1998).
38. M. Köhl, M. J. Davis, C. W. Gardiner, T. W. Hänsch, and T. Esslinger, "Growth of Bose–Einstein Condensates from Thermal Vapor," Phys. Rev. Lett. **88**, 080402 (2002).
39. M. J. Davis, T. M. Wright, T. Gasenzer, S. A. Gardiner, and N. P. Proukakis, "Formation of Bose–Einstein Condensates," in *Universal Themes of Bose–Einstein Condensation*, edited by N. Proukakis, D. Snoke, and P. Littlewood (Cambridge University Press, 2017).
40. J. Beugnon and N. Navon, "Exploring the Kibble–Zurek mechanism with homogeneous Bose gases," J. Phys. B: At. Mol. Opt. Phys. **50**, 022002 (2017).
41. A. L. Gaunt, T. F. Schmidutz, I. Gotlibovych, R. P. Smith, and Z. Hadzibabic, "Bose–Einstein Condensation of Atoms in a Uniform Potential," Phys. Rev. Lett. **110**, 200406 (2013).
42. C. Eigen, A. L. Gaunt, A. Suleymanzade, N. Navon, Z. Hadzibabic, and R. P. Smith, "Observation of Weak Collapse in a Bose–Einstein Condensate," Phys. Rev. X **6**, 041058 (2016).
43. S. Dyachenko, A. C. Newell, A. Pushkarev, and V. E. Zakharov, "Optical turbulence: weak turbulence, condensates and collapsing filaments in the nonlinear Schrödinger equation," Physica D **57**, 96–160 (1992).
44. N. Navon, A. L. Gaunt, R. P. Smith, and Z. Hadzibabic, "Emergence of a turbulent cascade in a quantum gas," Nature **539**, 72–75 (2016).
45. N. Navon, C. Eigen, J. Zhang, R. Lopes, A. L. Gaunt, K. Fujimoto, M. Tsubota, R. P. Smith, and Z. Hadzibabic, "Synthetic dissipation and cascade fluxes in a turbulent quantum gas," Science **366**, 382–385 (2019).
46. I. Gotlibovych, T. F. Schmidutz, A. L. Gaunt, N. Navon, R. P. Smith, and Z. Hadzibabic, "Observing properties of an interacting homogeneous Bose–Einstein condensate: Heisenberg-limited momentum spread, interaction energy, and free-expansion dynamics," Phys. Rev. A **89**, 061604 (2014).
47. C. N. Weiler, T. W. Neely, D. R. Scherer, A. S. Bradley, M. J. Davis, and B. P. Anderson, "Spontaneous vortices in the formation of Bose–Einstein condensates," Nature **455**, 948–951 (2008).
48. N. Navon, A. L. Gaunt, R. P. Smith, and Z. Hadzibabic, "Critical dynamics of spontaneous symmetry breaking in a homogeneous Bose gas," Science **347**, 167–170 (2015).

Methods

Additional state-preparation details. To prepare our far-from-equilibrium state, we lower U_D/k_B to 30 nK. Note that U_D caps the component of an atom's momentum perpendicular to any of the trap walls, and not its total momentum, so in the absence of collisions some atoms with energy exceeding U_D remain in the trap. After the high-energy atoms have left both the trap and the field of view, we raise U_D/k_B to 400 nK, sufficient to prevent evaporation while avoiding technical heating during thermalisation. Since the optical-box walls are not infinitely sharp[41], the effective D and L depend slightly on U_D and E; during thermalisation $D = 25(2)\,\mu$m and $L = 42(2)\,\mu$m.

Momentum distributions. We take absorption images of our clouds, after a time-of-flight (ToF) ballistic expansion of variable duration t_{ToF}, along the symmetry axis of our cylindrical box trap. For $2\hbar k t_{ToF}/m$ sufficiently larger than D and L, such images faithfully give the line-of-sight-integrated momentum distribution. To deduce n_k values that vary over 5 orders of magnitude (see Fig. 2) we combine data taken with various t_{ToF} in the range [10 ms, 80 ms]; the longest t_{ToF} is needed to minimise finite-size effects at low k, while shorter ones gives better signal-to-noise at large k. We always repeat measurements about 10 times under identical experimental conditions.

To reconstruct the 3D momentum distribution, we average our images azimuthally and perform the inverse-Abel transform. This assumes spherical symmetry, and in the paper we always treat n_k as dependent only on $k = |\mathbf{k}|$. For a fully coherent BEC the momentum distribution is not isotropic (but depends on the box shape), but this does not invalidate our definition of Δ_k in terms of the cumulative distribution F_k.

The theoretical prediction for the Heisenberg width $\Delta_k^H = 0.18(2)\,\mu\text{m}^{-1}$ in Fig. 4b is obtained by numerically finding the momentum distribution in the Gross–Pitaevskii ground state for our box, integrating along the imaging direction and performing the inverse-Abel transform; the uncertainty in the theoretical Δ_k^H accounts for both the weak dependence on a and the uncertainties in D and L. The value of Δ_k at long thermalisation times is also consistent with $0.21(2)\,\mu\text{m}^{-1}$ that we experimentally observe for a slowly prepared equilibrium gas. Also note that the theoretical Δ_k^H for a spherical box of equal volume is only slightly smaller, $\Delta_k^H = 0.15(2)\,\mu\text{m}^{-1}$.

Equilibrium temperature and condensate atom number. Within the ideal-gas approximation, in an equilibrium saturated Bose gas, with chemical potential $\mu = 0$, the total number of non-condensed atoms is

$$N_{th} = \frac{V}{(2\pi)^3}\int \mathrm{d}^3\mathbf{k}\,\frac{1}{\exp[\hbar^2k^2/(2mk_BT)]-1} = \zeta(\tfrac{3}{2})\frac{V}{\lambda^3},$$

and the total energy is

$$E = \frac{V}{(2\pi)^3}\int \mathrm{d}^3\mathbf{k}\,\frac{\hbar^2k^2/(2m)}{\exp[\hbar^2k^2/(2mk_BT)]-1} = \tfrac{3}{2}\zeta(\tfrac{5}{2})\frac{V}{\lambda^3}k_BT,$$

where $\zeta(3/2) \approx 2.612$ and $\zeta(5/2) \approx 1.341$ are values of the Riemann zeta function, and $\lambda = h/\sqrt{2\pi m k_B T}$ is the thermal wavelength. Note that the energy per thermal atom, $E/N_{th} \approx 0.77\,k_BT$, is lower than the equipartition-theorem result in a classical gas, because the degenerate-gas Bose distribution has a relatively larger population of low-energy states than the Boltzmann one (see ref. [49]).

In our isolated gas, $E = k_B \times 0.35(1)$ mK and the total particle number $N = 2.69(1) \times 10^4$ are fixed. From E we get the equilibrium $T = 32(2)$ nK, which then gives the equilibrium $N_{th} = 1.4(1) \times 10^4$ and the equilibrium condensate atom number $N_{QC} = N - N_{th} = 1.3(1) \times 10^4$.

Scaling exponents. We determine the optimal α and β using an F–statistic approach. For a given $\{\alpha, \beta\}$ pair, we calculate the variation between the scaled n_k curves taken for different t within the scaling interval, focusing on the relevant (IR or UV) momentum range. We compare this spread to the average experimental spread in the data taken for individual t values and find $\{\alpha, \beta\}$ that minimise the ratio of the two. We estimate the uncertainty in α and β by sampling 80 data subsets, each containing one third of the data, and use the spread of the obtained exponents. For additional details, see Extended Data Fig. 1.

Data availability

The data that support the findings of this study are available in the Apollo repository (https://doi.org/10.17863/CAM.53984). Any additional information is available from the corresponding authors on reasonable request.

References

49. T. F. Schmidutz, I. Gotlibovych, A. L. Gaunt, R. P. Smith, N. Navon, and Z. Hadzibabic, "Quantum Joule–Thomson Effect in a Saturated Homogeneous Bose Gas," Phys. Rev. Lett. **112**, 040403 (2014).

Acknowledgements

We thank J. Berges, T. Gasenzer, J. Schmiedmayer, M. K. Oberthaler, E. A. Cornell, V. Kasper, and N. Navon for discussions. This work was supported by EPSRC [Grants No. EP/N011759/1 and No. EP/P009565/1], ERC (QBox), and a QuantERA grant (NAQUAS, EPSRC Grant No. EP/R043396/1). C. E. acknowledges support from Jesus College (Cambridge). T. A. H. acknowledges support from the EU Marie Skłodowska-Curie program [Grant No. MSCA-IF-2018 840081]. R. P. S. acknowledges support from the Royal Society. Z. H. acknowledges support from the Royal Society Wolfson Fellowship.

Author contributions

J. A. P. G. led the project. L. H. D. and C. E. contributed significantly to data collection, analysis, and production of figures. All authors contributed extensively to interpretation of the data and production of the manuscript.

Competing interests

The authors declare no competing interests.

Additional information

Correspondence and requests for materials should be addressed to J. A. P. G. or Z. H.

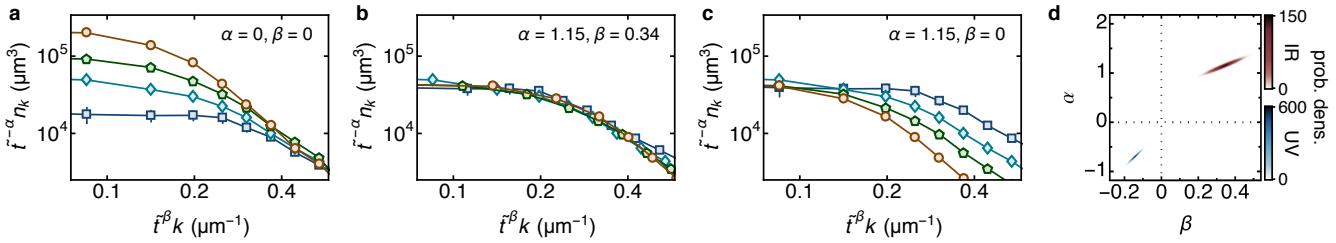

Extended Data Fig. 1 | Additional details of scaling procedure, for the $a = 300\,a_0$ data shown in Fig. 2 in the main text. **a-c,** IR scaling dynamics on log-log axes. Panels **a** and **b** correspond to the top and bottom panel, respectively, in Fig. 2c in the main text. In **c** we illustrate partial collapse, with $\alpha = 1.15$ and $\beta = 0$, to show more clearly how much the distribution moves along the k axis. **d,** Overview of scaling exponent probability densities for both IR and UV.